



Nogo-A/Pir-B/TrkB Signaling Pathway Activation Inhibits Neuronal Survival and Axonal Regeneration After Experimental Intracerebral Hemorrhage in Rats

Yinlong Liu¹ · Chao Ma² · Haiying Li² · Haitao Shen² · Xiang Li² · Xi'an Fu¹ · Jiang Wu² · Gang Chen²

Received: 16 January 2019 / Accepted: 25 June 2019
© Springer Science+Business Media, LLC, part of Springer Nature 2019

Abstract

Intracerebral hemorrhage (ICH) leads to widespread pathological lesions in the brain, especially impacting neuronal survival and axonal regeneration. This study aimed to elucidate whether the Nogo-A (a myelin-related protein)/paired immunoglobulin-like receptor B (Pir-B)/tropomyosin receptor kinase B (TrkB) pathway could exert a regulatory effect in ICH. An ICH model was first established in Sprague Dawley rats, followed by different administrations of vehicle, k252a, or NSC 87877. The Morris water maze test was performed to observe ICH-induced cognitive dysfunction in rats. Rats in the ICH + NSC 87877 group showed better cognitive performance compared with those injected with vehicle or k252a. Neurobehavioral scores were identical. By harvesting brain tissues at different time points after ICH, we detected the expression levels of Nogo-A and PirB with western blot and immunofluorescence and found that they were markedly upregulated at 48 h after ICH. TUNEL and Fluoro-Jade B staining showed that NSC 87877 treatment attenuated ICH-induced apoptosis and neuronal death, whereas k252a treatment aggravated these pathological changes. The expression levels of growth-associated protein 43 (GAP43) and neurofilament 200 (NF200) were higher in the ICH + NSC 87877 group compared with the ICH + vehicle group, but were lower in the ICH + k252a group. Finally, we confirmed the protective role of p-TrkB/TrkB in ICH by western blot. To sum up, our study identified the inhibitory role of the Nogo-A/PirB/TrkB pathway in ICH; however, p-TrkB/TrkB may serve as a potential target for secondary brain injury post-ICH.

Keywords Intracerebral hemorrhage · Nogo-A · Tropomyosin receptor kinase B · Axonal regeneration · Neuron cell death · Growth-associated protein 43

Introduction

Intracerebral hemorrhage (ICH) is a pathological condition of primary nontraumatic ICH, accounting for 10–30% of all stroke cases (Hijioka et al. 2017). Hypertension is the most

common pathogenesis of ICH. The peak period of brain edema subsequently occurs at 48 h after ICH, severely aggravating the clinical symptoms and signs (Lei et al. 2016). Bleeding or edema causes compression of brain tissues, which will further lead to secondary neurological deficits that are difficult to recover, seriously affecting the prognosis and life quality of ICH patients. Currently, only about 20% of ICH patients are capable of recovering functional independence within 6 months post-ICH (Urday et al. 2015; Xi et al. 2014). Hence, comprehensive explorations of the mechanism of ICH are urgently needed in order to improve the therapeutic efficacy and clinical outcomes of ICH.

Axons are neuronal output channels that transmit cellular nerve impulses to other neurons or effectors distributed in muscles and glands (Wilson 2018). In the nervous system, axons are the main signaling channel (Banerjee et al. 2018; Eyal et al. 2018). The axons and the cell bodies of neurons form a structural and functional entirety. Substances that are metabolized by neurons within 6 months post-ICH are mostly

Yinlong Liu and Chao Ma contributed equally to this work.

✉ Xi'an Fu
cowankang@126.com

✉ Jiang Wu
wujiangsz@163.com

¹ Department of Neurosurgery, The Affiliated Suzhou Hospital of Nanjing Medical University, Suzhou Municipal Hospital, 242 Guangji road., Suzhou 215008, Jiangsu Province, China

² Department of Neurosurgery & Brain and Nerve Research Laboratory, The First Affiliated Hospital of Soochow University, 188 Shizi Street, Suzhou 215006, Jiangsu Province, China

formed in the cell body. The metabolism of the overall physiological activity of neurons is realized by the continuous flow of axoplasm. Post-ICH, compression of the hematoma or cerebral edema causes the release of thrombin, bilirubin, and other toxic substances in surrounding tissues of the lesion sites. In addition, blood–brain barrier damage further aggravates brain edema (Wang et al. 2017), which in turn causes damage to nerve fibers and axons. Related research has found that glial scar formation, neurotrophic factor deficiency, and release of axonal regeneration inhibitors remarkably limit axon regeneration, which is the main reason for the difficulty in recovery of nerve function after ICH (Jeong et al. 2012; Karuppagounder et al. 2016).

A myelin-related protein, Nogo-A derived from myelin-associated inhibitors (MAIs) is a crucial inhibitor found in the central nervous system (CNS), exerting axonal growth inhibition through its neuronal receptor, paired immunoglobulin-like receptor B (PirB), after CNS injury (Akbik et al. 2012; Yiu and He 2006), and inhibition of the PirB signaling cascades in neurons enhances axon regeneration after optic nerve injury in mice (Fujita et al. 2011). Tropomyosin receptor kinase B (TrkB) belongs to the receptor tyrosine protein kinase family and is a specific receptor for brain-derived neurotrophic factor (BDNF) (Osborne et al. 2018). Binding of BDNF to the TrkB receptor on the target cell membrane enhances the degree of autophosphorylation of tyrosine receptor residues in the cell region of the TrkB receptor, which in turn activates a cascade of downstream tyrosine phosphorylation (Naylor et al. 2002). Previous studies mainly focused on the potential roles of TrkB in regulating tumor development (Allen et al. 2018; Meldolesi 2018). Several Trk-targeting compounds are in clinical development, showing encouraging activities and durable responses in tumor patients. Interestingly, phosphorylation of TrkB may be associated with depression or depression-like behavior and dendritic changes in mice after inflammation (Zhang et al. 2014), and ω -3 polyunsaturated fatty acids (ω -3PUFAs) enhance the TrkB pathway by activating extracellular signal-regulated protein kinases (ERK) and AKT/protein kinase B, thereby increasing the synaptic plasticity and decreasing neuron loss in schizophrenic rats (Fang et al. 2017). Fujita et al. found that binding of myelin-associated glycoprotein (MAG) to PirB led to the association of PirB with tropomyosin receptor kinase (Trk) neurotrophin receptors, and phosphorylation of TrkB improved axon regeneration after optic nerve injury (Fujita et al. 2011). Therefore, in recent years, the biological functions of TrkB in axonal elongation and regeneration have attracted attention in post-ICH treatment. So far, the specific effect of Nogo-A on the CNS has not been fully explored.

In the present study, we aimed to elucidate whether Nogo-A could inhibit the activation of p-TrkB/TrkB and contribute to the regulation of secondary brain injury (SBI) post-ICH. We focused on the effects of the Nogo-A/PirB/TrkB pathway on

neuronal cell death, functional deficits, and axonal regeneration after ICH, providing a theoretical basis for SBI. A better understanding of the Nogo-A/PirB/TrkB pathway function and mechanisms after ICH may provide insight into novel therapeutic targets for the treatment of ICH injury.

Materials and Methods

Experimental Animals

Eight-week-old male (250–300 g) Sprague Dawley (SD) rats provided by the Shanghai Experimental Animal Center of the Chinese Academy of Sciences were selected for use in this study. Each rat was individually housed in an environment with a temperature of 18–22 °C and relative humidity of 40–70% under a regular light/dark schedule. Food and water were available ad libitum. Sample sizes were determined by power analysis during the animal ethics dossier application. All procedures were approved by the Animal Protection Committee of Soochow University and were performed in accordance with the National Institutes of Health's guidelines on the care and use of animals and the Animal Research: Reporting In Vivo Experiments guidelines (National Research Council 2011). All efforts were made to minimize animal suffering and the number of animals used. For details, please refer to the National Research Council (2011) Guide for the Care and Use of Laboratory Animals (National Academies Press, 8th Ed., Washington, DC) (National Research Council 2011).

Establishment of Experimental ICH Model in Rats

A collagenase ICH model was constructed as previously reported (Wang et al. 2017). Briefly, rats were anesthetized (4% chloral hydrate, 10 ml/kg, intraperitoneal injection) and fixed in a stereotactic apparatus (ZH-Lanxing B-type stereotaxic frame, Anhui Zhenghua Biological Equipment Co. Ltd., Anhui, China). Subsequently, the right striatum of the rat was slowly (5 min) unilaterally injected with 0.23 U collagenase VII infused with 1 μ l physiological saline solution. Rats in the sham group were injected with an equal-volume physiological saline solution. A schematic representation of the brain coronal sections is shown in Fig. 1a.

Experiment Grouping

Part 1: Time Course Analysis of the Protein Levels of Nogo-A and PirB After ICH

For the in vivo experiment, a total of 50 rats (48 of which survived the experiment) were selected and assigned into eight groups, with six rats in each group. All rats except those in the sham group underwent the ICH procedure. The rats were

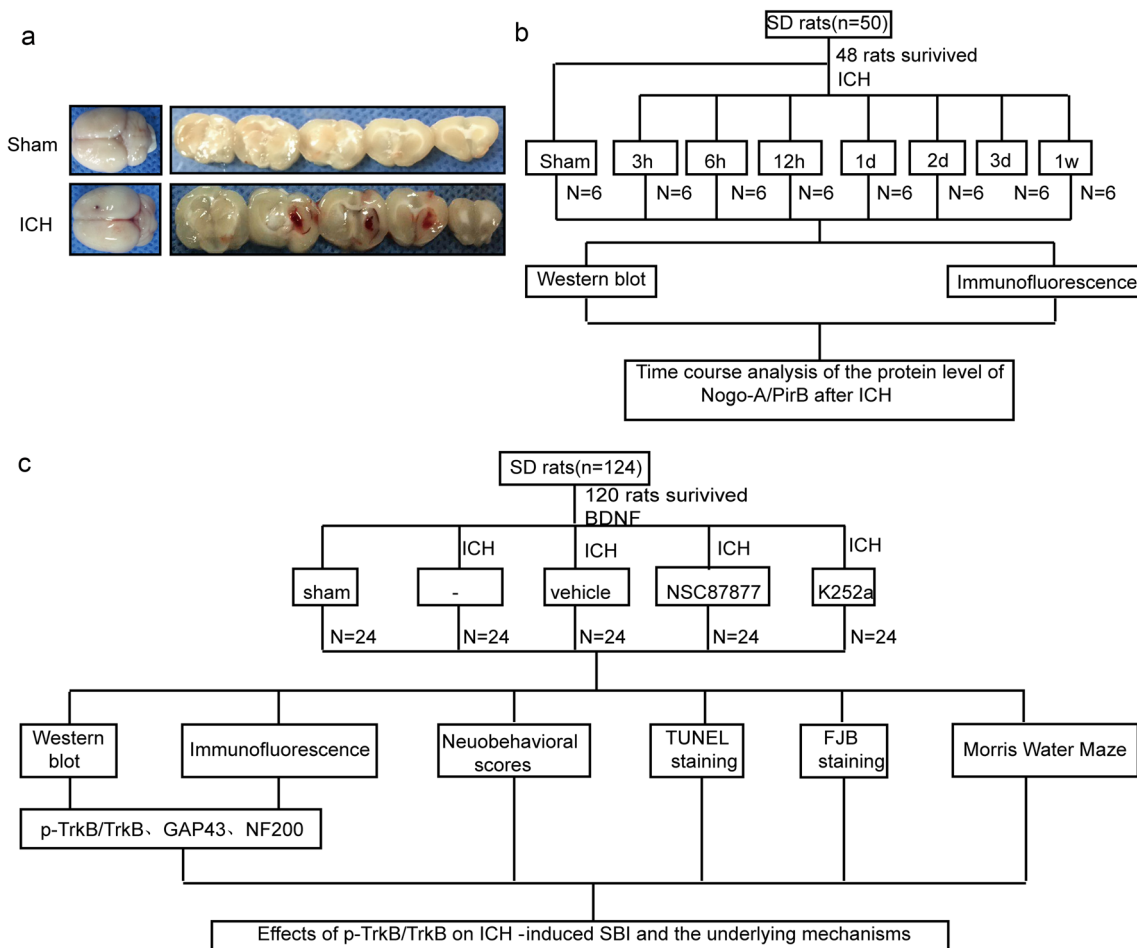


Fig. 1 Construction of the ICH model in rats. **a** Rat brains extracted from the sham group and post-ICH at 3 h, 6 h, 12 h, 1 day, 2 day, 3 day, and 1 week. **b** Time course analysis of the protein levels of Nogo-A/PirB/

TrkB after ICH. **c** Effects of p-TrkB/TrkB on ICH-induced SBI and the underlying mechanism. NSC 87877: 2.5 ng/μl, i.c.v.; K252a: 100 nM, i.c.v.

sacrificed at 3 h, 6 h, 12 h, 24 h, 48 h, 72 h, or 1 week after the ICH or sham procedure according to their specific grouping. The rat brain cortex was harvested for the subsequent western blot and immunofluorescence (Fig. 1b). To avoid potential red blood cell contamination, the tissue was sampled 1 mm away from the hematoma.

another 6 rats per group were subjected to neurological impairment evaluation at 1 week after ICH; and the last 12 rats in each group were subjected to the Morris water maze test at 12 days after ICH (Fig. 1c).

Part 2: Effects of Nogo-A/PirB/TrkB Pathway on ICH-Induced SBI and Its Underlying Mechanisms

A total of 124 rats injected with BDNF (5 μg/μl) intracerebroventricularly (120 of which survived the experiment) were randomly assigned into the sham group, ICH group, ICH + vehicle group, ICH + NSC 87877 group (NSC 87877, 2.5 ng/μl, into cerebral ventricles), and ICH + K252a group (K252a, 100 nM, into cerebral ventricles). Each group contained 24 rats. At 48 h after ICH, the brains of 6 rats per group were extracted for western blot, Nissl staining, terminal deoxynucleotidyl transferase-mediated dUTP nick end labeling (TUNEL) staining, and Fluoro-Jade B (FJB) staining;

Reagents and Antibodies

The following reagents were used in this study: recombinant rat BDNF (450–02, 100 ng/ml; PeproTech, Rocky Hill, NJ, USA), NSC 87877 (S8182, Selleck Chemicals, USA), and K252a (SF2370, 100 nM; Alomone Labs, Jerusalem, Israel). Anti-Nogo-A (CST13401, RRID: AB_2798209) and anti-phosphoTrkB (CST4619, RRID:AB_10235585) were purchased from Cell Signaling Technology (Danvers, MA, USA); anti-PirB (AF2754, RRID:AB_2249965) was purchased from R&D Systems (Minneapolis, MN, USA); anti-TrkB (ab18987, RRID:AB_444716), anti-GAP43 (ab16053, RRID:AB_443303), and anti-NF200 (ab82259, RRID:AB_1658500) were purchased from Abcam (Cambridge, MA, USA); anti-β-tubulin (sc-9140,

RRID:AB_2187342), goat anti-rabbit IgG-HRP (sc-2004, RRID:AB_631746), and goat anti-mouse IgG-HRP (sc-2005, RRID:AB_631736) were purchased from Santa Cruz Biotechnology (Santa Cruz, CA, USA); Alexa Fluor 555 donkey anti-rabbit IgG antibody (A31572, RRID:AB_162543), Alexa Fluor 488 donkey anti-mouse IgG antibody (A21202, RRID:AB_141607), Alexa Fluor 488 donkey anti-goat IgG antibody (A21206, RRID:AB_2535792), and Alexa Fluor 555 donkey anti-mouse IgG antibody (A31570, RRID:AB_2536180) were purchased from Invitrogen (Carlsbad, CA, USA).

Western Blot

Tissues were lysed with RIPA lysis buffer in the presence of a protease inhibitor (Sigma-Aldrich, St. Louis, MO, USA) to harvest total cellular protein. The protein concentration of each cell lysate was quantified using a bicinchoninic acid (BCA) protein assay kit (Pierce, Rockford, IL, USA). An equal amount of protein sample was loaded onto a 10% sodium dodecyl sulfate-polyacrylamide gel electrophoresis (SDS-PAGE) gel and then transferred to a polyvinylidene fluoride (PVDF) membrane after being separated. After blockage with skim milk, membranes were incubated with primary and secondary antibody and subsequently revealed with an enhanced chemiluminescence detection kit. The relative quantity of proteins was analyzed by ImageJ and normalized to that of loading controls. The quantitative analysis was performed by observers who were blind to the experimental groups.

Immunofluorescence

Rat brain tissues were fixed in 4% paraformaldehyde overnight; the fixed time usually do not exceed 18 h (the longer the fixed time, the more serious the tissue antigen loss). It is advisable to control the fixed time within 12 h in general. Rat brain tissues were washed with water and then hydrated (50% ethanol for 25 min, 70% ethanol for 25 min, 80% ethanol for 25 min, 90% ethanol for 25 min, 95% ethanol I for 10 min, 95% ethanol II for 15 min, 100% ethanol I for 10 min, 100% ethanol II for 15 min, xylene I for 15 min, xylene II for 15 min). Then, the brain tissues were immersed in paraffin liquid for 6 h, and then the paraffin was poured into the embedding tank. The brain tissues immersed in the paraffin was removed, and the brain tissues were clamped with small tweezers and placed in the central part of the depression of the embedding tank. The embedded wax block could be separated from the embedding tank after sitting for at least 30 min, and cut into 4- μ m sections, which were dewaxed immediately before immunofluorescence staining. Incubation of the primary and secondary antibodies was conducted in the dark. To exclude the false binding of the secondary antibodies, a “wrong” secondary antibody was used as a negative control

(data not shown). Tissues were stained with DAPI and observed by a fluorescence microscope (Olympus BX50/BX-FLA/DP70, Olympus Co., Japan) or a laser scanning confocal microscope (ZEISS LSM 880, Carl Zeiss AG, Germany). Finally, six random sections from each sample were examined, and representative results were shown.

Behavior Testing

According to a previous study (Wang et al. 2013), spatial learning and memory were evaluated with the Morris water maze, including the cued learning procedure, spatial acquisition task, reference memory task, and working memory task. At day 12, rats were trained for the Morris water maze test for five consecutive days until day 16. Briefly, the apparatus consisted of a circular pool (200 cm diameter \times 75 cm height \times 40 cm depth) containing water with a temperature of 23 ± 2 °C. Nontoxic blue paint was added to the water. Four equidistant points, N, E, S, and W, were marked on the wall of the pool as the starting point of the experiment, dividing the pool into four quadrants. Rats were pretreated on the visible platform. During the formal experiment, the platform was removed and rats were released into the pool from the opposite side of the original platform location. The swimming path was recorded for 60 s of each trial (Polytrack System, San Diego Instruments, San Diego, CA, USA). Escape latency (s) and swimming distance (cm) were recorded four times per day.

Neurological Impairment

At 1 week after ICH surgery, SD rats were examined for behavioral impairment with a scoring system and monitored for activity, appetite, and neurological defects as described previously (Li et al. 2018) (Table 1).

Nissl Staining

Paraffin-embedded rat brain tissues were dewaxed, stained with 5% toluidine blue at room temperature for 10 min, and

Table 1 Behavior and activity scores

Category	Behavior	Score
Appetite	Finished meal	0
	Left meal unfinished	1
	Scarcely ate	2
Activity	Walk and reach at least three corners of the cage	0
	Walk with some stimulations	1
	Almost always lying down	2
Deficits	No deficits	0
	Unstable walk	1
	Impossible to walk	2

rinsed in 95% ethanol, and dimethylbenzene (Sigma-Aldrich). Finally, slides were sealed with neutral balsam and captured using the fluorescence microscope (Olympus BX50/BX-FLA/DP70; Olympus Co.).

FJB and TUNEL Staining

FJB and TUNEL staining was performed as described previously (Shen et al. 2015). Briefly, paraffin-embedded rat brain tissues were dewaxed, TUNEL staining was performed using the In Situ Cell Death Detection Kit (Roche, 11684795910). Brain sections were observed under a fluorescence microscope, and ImageJ software was used to analyze TUNEL staining. For FJB staining, the sections were incubated with 0.06% KMnO_4 solution and then were incubated with FJB working solution (containing 0.1% acetic acid). Finally, brain sections were observed under a fluorescence microscope, and ImageJ software was used to analyze the positive rate of FJB. The quantitative analysis was performed by an observer who was blind to the experimental groups.

Statistical Processing

Datasets are detected by both Shapiro–Wilk normality test and KS normality test to check whether they adhered to a Gaussian distribution. Data with normal distribution are presented as mean \pm SEM (except the neurobehavioral scores). GraphPad Prism 5 (GraphPad Software, La Jolla, CA, USA) was used for all statistical analyses. One-way ANOVA for multiple comparisons and the Student–Newman–Keuls post hoc test were used to determine the differences among all groups. Neurobehavioral scoring is presented as the median with the interquartile range. $P < 0.05$ was considered to be a significant difference.

Results

The Protein Levels of Nogo-A and PirB Were Elevated After ICH

Regeneration after ICH-induced impairment is difficult to achieve, mainly due to the weak regeneration ability of terminal differentiated neurons, lack of neurotrophic factors, and axonal growth inhibition. Nogo-A and PirB, as crucial factors in inhibiting axon regeneration, were markedly upregulated after ICH until day 2 and then gradually decreased at day 3 and day 7 in brain tissues of ICH rats (Fig. 2a and b). Similarly, immunofluorescence results revealed higher abundance of PirB in ICH mice compared with the sham group (Fig. 2c). The brain tissue harvested after animal procedures clearly showed hemorrhage in ICH rats, suggesting the successful construction of the ICH model in rats (Fig. 1a). Here,

we observed that the expression of both Nogo-A and PirB peaked at 48 h, suggesting that the SBI was the most pronounced at this time point.

Nogo-A/PirB/TrkB Activation Inhibited Cognitive Impairment After ICH in Rats

It has been reported that cognitive, memory, and learning functions are impaired post-ICH. We performed the Morris water maze test to evaluate the cognitive impairment in rats. Here, k252a (a pan-Trk inhibitor, activating the Nogo-A/PirB/TrkB pathway) or NSC 87877 (Src homology 2-containing protein tyrosine phosphatase 1/2 inhibitor, inhibiting the Nogo-A/PirB/TrkB pathway) was applied. By comparison, ICH rats showed a path that was distributed among all quarters randomly. Among the four groups with ICH procedures, rats in the ICH + K252a group showed the most distributed swimming path, whereas those in the ICH + NSC 87877 group swam along a relatively random path within the quadrants (Fig. 3a). Subsequently, escape latency and swimming distance were assessed to evaluate the cognitive impairment after ICH. As shown in Fig. 3 b and c, ICH rats presented higher escape latency than those in the sham group from day 12 to day 16 ($P < 0.01$). Consistently, the average swimming distance was the shortest in the sham group from the 12th day to the 16th day (Fig. 3d and e, $P < 0.01$). These data confirmed the impaired cognitive function in post-ICH rats. It is noteworthy that K252a administration aggravated cognitive function, showing the opposite effect of NSC 87877 administration. These results indicate that Nogo-A/PirB/TrkB pathway activation aggravates the behavioral and cognitive dysfunction after ICH, while inhibiting the pathway can improve it.

Nogo-A/PirB/TrkB Activation Aggravated Apoptosis and Neuronal Death After ICH in Rats

We performed Nissl staining to examine the survival of neurons in the rat cortex and CA1 region. All four ICH groups presented fewer Nissl-positive neurons in the cortex and CA1 region compared with the sham group. In particular, the ICH + K252a group had the lowest staining of Nissl-positive neurons, indicating the most severe neuronal death among the five groups. NSC 87877 treatment significantly increased the rate of neuron survival, but it was still lower than that of the sham group ($P < 0.05$, Fig. 4a–c). Likewise, neurobehavioral scores indicated that NSC 87877 markedly elevated neuronal behaviors post-ICH (Fig. 4d). Together, the above findings demonstrated the protective effect of NSC 87877 on ICH rats.

To evaluate ICH-induced cell necrosis, we harvested rat cortex and perihematoma tissues in each group. FJB staining revealed abundant necrotic cells (white arrows) in both cortex and perihematoma tissues compared with the sham group.

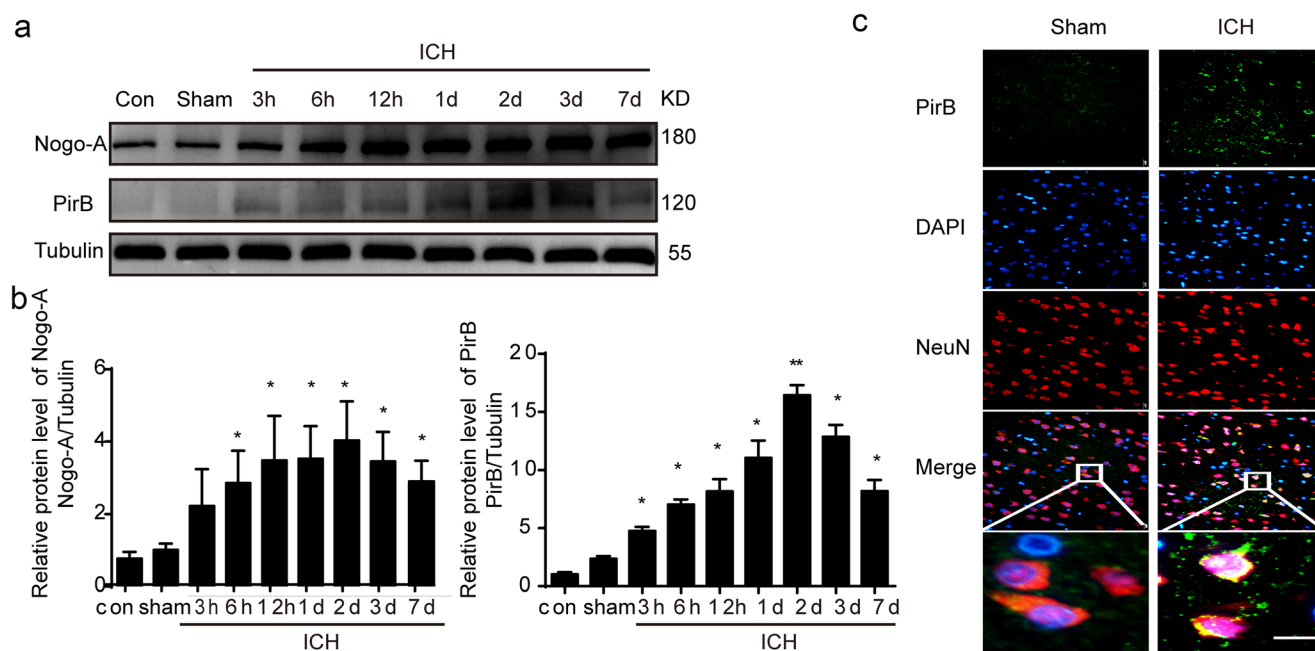


Fig. 2 The protein levels of Nogo-A and PirB were elevated after ICH in the rat brain. **a** Protein levels of Nogo-A and PirB in rat brains of different groups. Tubulin served as the loading control. **b** Relative protein levels of Nogo-A/tubulin and PirB/tubulin in the rat brain. * $P < 0.05$, ** $P < 0.01$

compared with the sham group. **c** Immunofluorescence analyses of PirB (green), nucleus stained as DAPI (blue), and neurons (red). Scale bar = 100 μm

Compared with the ICH + vehicle group, a large number of necrotic cells were found in the K252a group, but NSC 87877 treatment markedly alleviated ICH-induced necrosis ($P < 0.05$, Fig. 5a–c). Subsequently, a TUNEL assay was conducted to elucidate the potential effects of NSC 87877 and K252a on ICH-induced neuronal apoptosis. The ICH groups showed abundant apoptotic neurons compared with the sham group. It is noteworthy that the NSC 87877 treatment group showed a lower percentage of apoptotic neurons than the ICH + vehicle group, and the ICH + K252a group exhibited the highest percentage of apoptotic neurons among the five groups ($P < 0.05$, Fig. 5d and e). In sum, Nogo-A/PirB/TrkB signaling pathway activation could aggravate apoptosis and neuronal death after ICH.

Nogo-A/PirB/TrkB Signaling Pathway Activation Inhibited Axon Regeneration After ICH

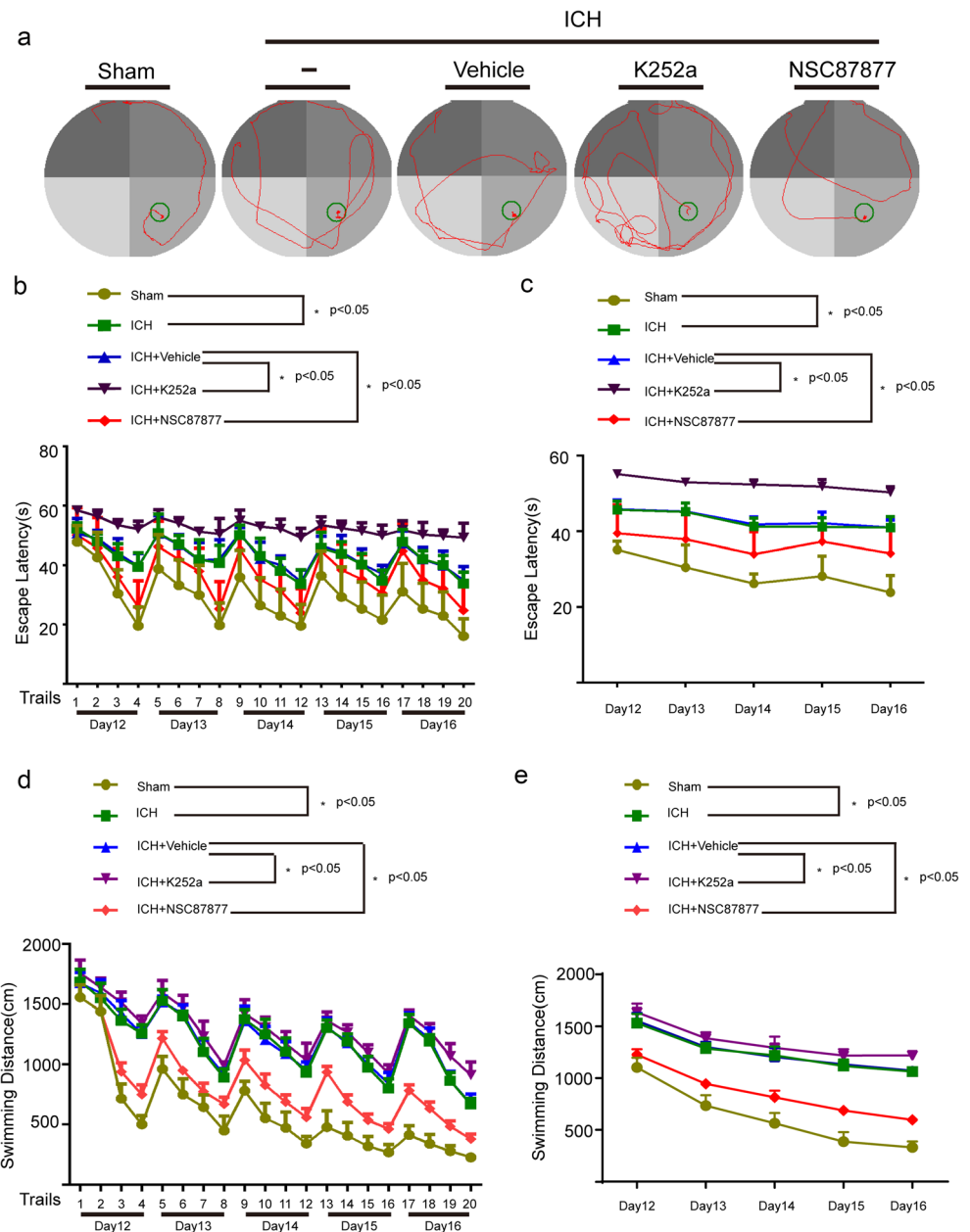
The Nogo-A signaling pathway is involved in axon regeneration (Akbik et al. 2012). To explore the mechanisms whereby NSC 87877 and K252a could influence neuronal behaviors, we mainly focused on the effects of Nogo-A/PirB/TrkB on axon regeneration post-ICH. According to previous reports, the upregulation of Nogo-A can indirectly downregulate the phosphorylation of TrkB (Akbik et al. 2012; Fujita et al. 2011). Furthermore, Trk receptors are completely inactive in the absence of neurotrophins and are difficult to detect (Osborne et al. 2018). Here, BDNF was supplied to raise the detection threshold. We determined the protein levels of TrkB

and the phosphorylation levels of TrkB (Tyr516) in brain tissues extracted from the five groups. As seen in Fig. 6a and b, the BDNF supply markedly activated TrkB and p-TrkB in ICH rats, indicating the potential role of p-TrkB/TrkB post-ICH. Moreover, the regulatory effects of NSC 87877 and K252a on the protein levels of TrkB and p-TrkB in the presence of BDNF were assessed. A higher relative protein level of p-TrkB/TrkB was observed in the ICH + NSC 87877 group than in the ICH + vehicle group. On the contrary, K252a treatment resulted in downregulated p-TrkB/TrkB (Fig. 6c and d). As crucial factors in axon growth, growth-associated protein 43 (GAP43) and neurofilament 200 (NF200) have been reported to be highly expressed during neuronal development and regeneration (Naylor et al. 2002). In the present study, western blot and immunofluorescence results both showed upregulated GAP43 and NF200 in the ICH + NSC 87877 group, which were remarkably downregulated by K252a treatment (Fig. 6e–g). Therefore, the activation of the inhibitory effect of the Nogo-A/PirB/TrkB signaling pathway on axon regeneration could be one of the main causes of aggravation of cognitive impairment and neuronal death after ICH.

Discussion

Globally, there are approximately 15 million stroke patients annually; among them, ICH accounts for 15% of all stroke cases (Lan et al. 2017). The ultrastructural pathology of ICH

Fig. 3 Nogo-A/PirB/TrkB activation inhibited cognitive impairment after ICH in rats. **a** Representative images of swimming paths of rats in each group. **b** Escape latency (s) of rats in each group. Data were recorded from day 12 to day 16, with four trails per day. * $P < 0.01$, ICH group compared with the sham group; * $P < 0.01$, ICH + K252a group compared with the ICH + vehicle group. **c** Average escape latency (s) of rats in each group. Data were recorded as the mean value from day 12 to day 16 with four trails per day. * $P < 0.01$, ICH group compared with the sham group; * $P < 0.01$, ICH + K252a group and ICH + NSC 87877 group compared with the ICH + vehicle group. **d** Swimming distance (cm) of rats in each group. Data were recorded from day 12 to day 16, with four trails per day. * $P < 0.01$, ICH group compared with the sham group; * $P < 0.01$, ICH + K252a group and ICH + NSC 87877 group compared with the ICH + vehicle group. **e** Average swimming distance (cm) of rats in each group. Data were recorded from day 12 to day 16, with four trails per day. * $P < 0.01$, ICH group compared with the sham group; * $P < 0.01$, ICH + K252a group and ICH + NSC 87877 group compared with the ICH + vehicle group



includes various factors. Among them, axonal damage and the subsequent regeneration are the major factors in ICH pathology, and more importantly, they are greatly involved in the long-term functional outcomes (Shen et al. 2015; Zhu et al. 2018). We believe that the improvement of axonal regeneration post-ICH could greatly contribute to the regaining of function in ICH patients.

The expression levels of Nogo-A and its receptors are up-regulated after ICH, indicating their potential roles in the pathological progression of ICH (Wang et al. 2007). Inhibition of Nogo-A activity by neutralizing protein after stroke markedly promotes regeneration of the corticospinal tract and restoration of neurological function (Tsai et al. 2007). If it is possible to reduce the intrinsic inhibitors mediated by Nogo-A and its

receptors, this may have a positive effect on the recovery of neurological function after ICH. PirB is highly expressed in the impaired nervous system and exerts an inhibitory effect on axonal regeneration. A previous study reported that PirB exerts negative regulation on axonal regeneration in the visual cortex (Syken et al. 2006). Similar results were also observed in our in vivo ICH model. In the present study, we observed that Nogo-A and PirB were markedly upregulated after ICH until day 2. Brain-derived neurotrophic factors exert key roles in synaptic plasticity, neurodevelopment, and neuroprotection through activation of NMDA receptors in the hippocampus. They bind to the myosin-related kinase B (TrkB) receptor, activate intracellular signaling pathways, and enhance synaptic strength to improve learning and memory functions (Li and

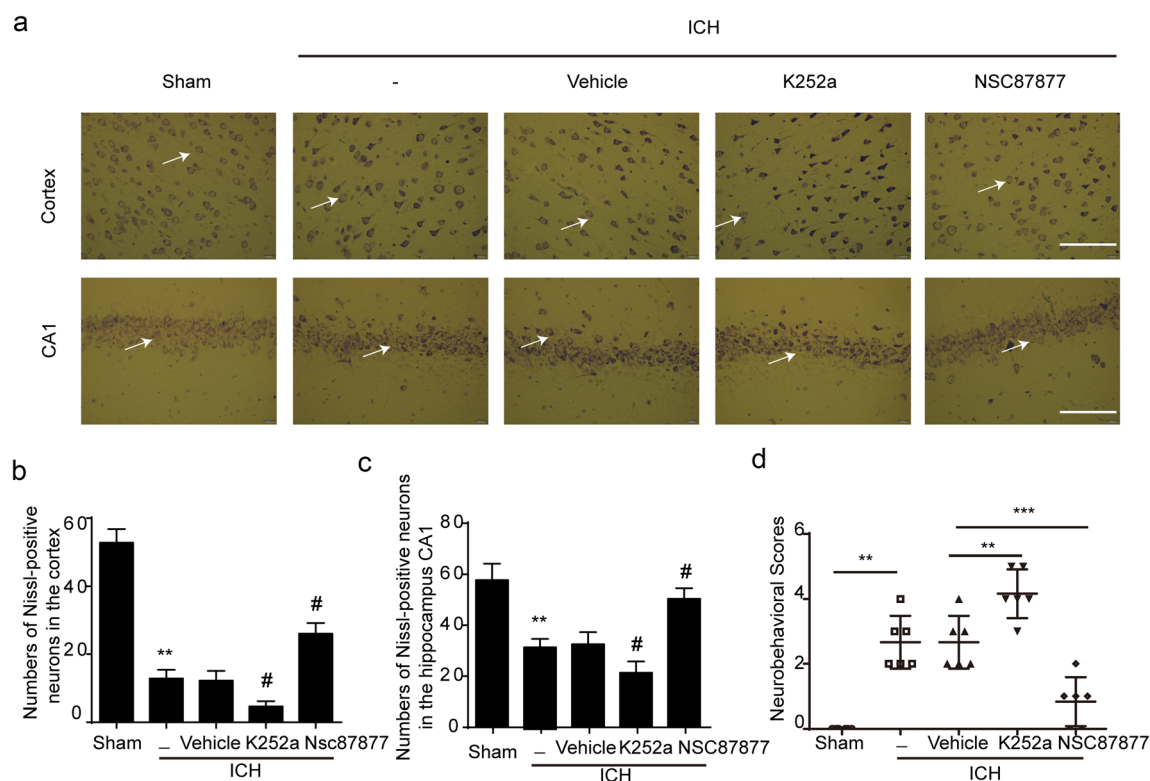


Fig. 4 Nogo-A/PirB/TrkB activation aggravated apoptosis and neuronal death after ICH in rats. **a** Nissl staining in the cortex and CA1 region of rats in different groups. Nissl-positive neurons were stained blue, as indicated by the white arrow. Scale bar = 100 μ m. **b**, **c** Numbers of Nissl-positive neurons in the cortex (**b**) and CA1 regions (**c**). ** P < 0.01, ICH group compared with the sham group; # P < 0.05, ICH

+ K252a group and ICH + NSC 87877 group compared with the ICH + vehicle group. (**d**) Neurobehavioral scores of each group. ** P < 0.01, ICH group compared with the sham group; * P < 0.05, ** P < 0.01, *** P < 0.001, ICH + K252a group and ICH + NSC 87877 group compared with the ICH + vehicle group

Liu 2010). A previous study found that the number of neural stem cells differentiated into oligodendrocytes after SHP2 knockout was significantly reduced (Ehrman et al. 2014). Yuki et al. (Fujita et al. 2011) suggested that SHP2 serves as a Trk tyrosine phosphatase; they confirmed that dephosphorylation of Trk receptors is reduced and the inhibitory effect of MAG on neurite growth is abolished by SHP2 inhibition. To investigate whether the Nogo-A/PirB/TrkB pathway may participate in the regulation of ICH, k252a (a pan-Trk inhibitor) or NSC 87877 (SHP1/SHP2 inhibitor) were used to intervention on ICH rats. Our study found that k252a showed pronounced neurobehavioral damage, whereas NSC 87877 treatment could remarkably attenuate ICH-induced cognitive dysfunction.

Besides the in vivo damage that ICH results, multiple cellular changes also occur post-ICH, including neuronal edema, swelling of neuronal axons and bulges, neuronal apoptosis, and necrosis. Abundant neuronal apoptosis and necrosis were seen in the brains of ICH rats in this study, especially in the ICH + k252a group. The ICH + NSC 87877 group showed fewer apoptotic and necrotic neurons after ICH, although the number was, unfortunately, still not reversed to the baseline. Based on the above findings, we hypothesized that Trk

inhibition aggravated ICH-induced cognitive function in rats as well as neuronal apoptosis and necrosis in the hematoma tissues. However, how the Nogo-A/PirB/TrkB pathway aggravates ICH in rats still remains unclear.

In the following experiments, we observed downregulated protein expression of GAP43 (growth-associated protein 43) and decreased NF200 (neurofilament 200)-positive nerve fibers in the brain tissues of ICH rats. GAP43 is a neuron-specific protein that is enriched in the axonal growth cone membrane and serves as a molecular marker for axonal regeneration. NF200 is a type of neurofilament protein, which provides elasticity to make nerve fibers easy to stretch and keep them from breaking down. A number of studies have detected the expressions of GAP43 and NF200 to reveal the condition of neurite outgrowth. Tan et al. (2017) suggested that higher expression levels of GAP43 and NF200 were expected to result in a better neurite outgrowth. Western blot and immunofluorescence results from another study showed robust expressions of neural markers in the generation of neural cells, including GAP43 and NF200 (Zhou et al. 2017). It is remarkable that NSC 87877 treatment in ICH rats obviously upregulated the expression levels of both GAP43 and NF200, whereas k252a invention presented the opposite trend. We

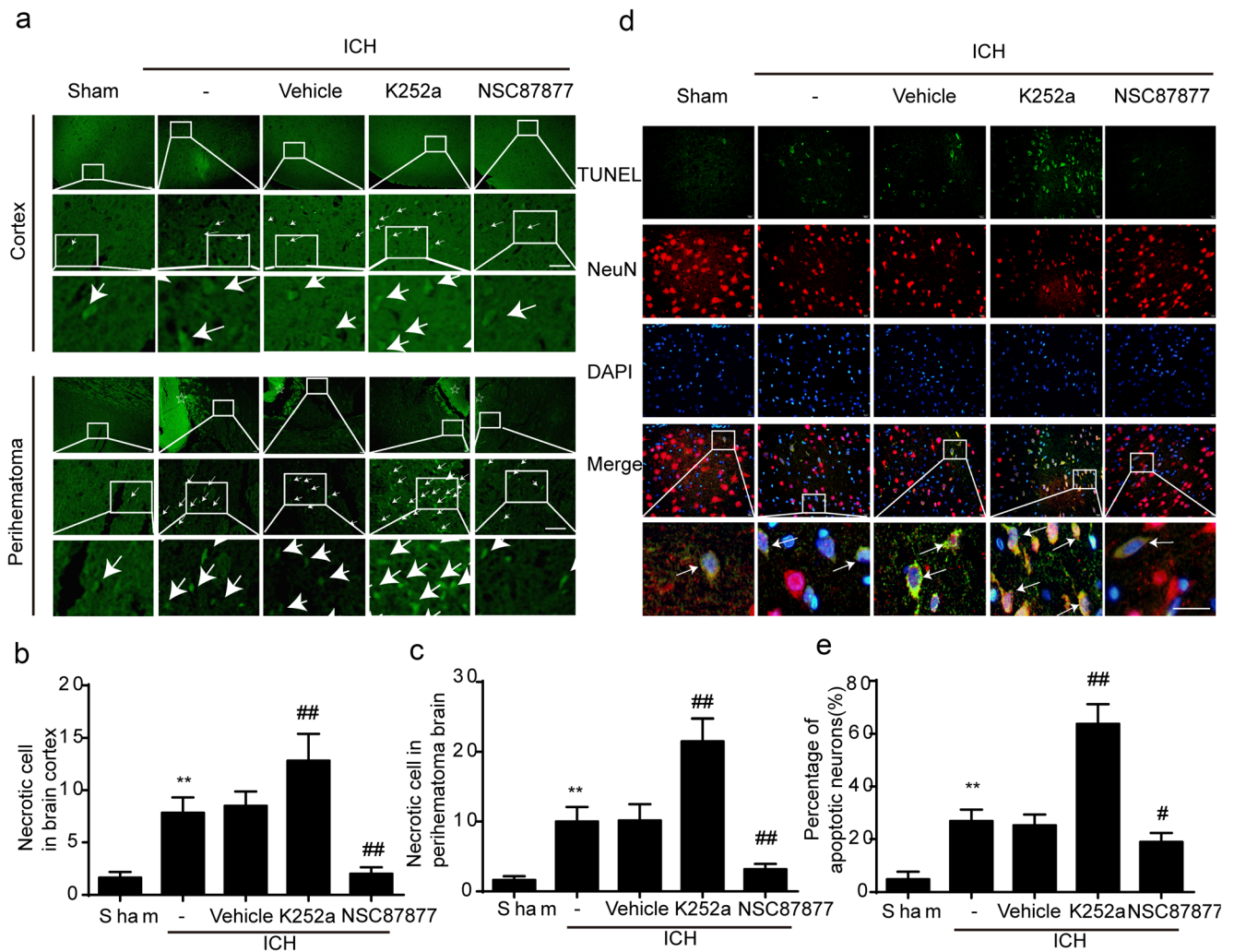


Fig. 5 NSC 87877 rescued and K252a aggravated apoptosis and neuronal death post-ICH at 2 day in vivo. **a** FJB staining (white arrow) in the rat cortex and perihematoma tissues of different groups. Neuronal degradation was stained as green. Scale bar = 100 μ m. **b, c** Quantification of neuronal degradation in the rat cortex (**b**) and perihematoma tissues (**c**). ****** $P < 0.01$, ICH group compared with the sham group; **###** $P < 0.01$, ICH + K252a group and ICH + NSC 87877 group compared with the ICH +

vehicle group. **d** TUNEL staining of apoptotic neurons in rat brains of different groups. Apoptotic neurons were stained green, neurons were stained red, and nuclei were stained blue as DAPI. Scale bar = 100 μ m. **e** Percentage of apoptotic neurons. ****** $P < 0.01$, ICH group compared with the sham group; **###** $P < 0.01$, ICH + K252a group and ICH + NSC 87877 group compared with the ICH + vehicle group

then demonstrated that Nogo-A/PirB/TrkB signaling pathway activation aggravated ICH-induced neurological changes through inhibiting neurite outgrowth, which was consistent with previous studies (Song et al. 2015).

Neural stem cells can proliferate and differentiate into neurons and glial cells under certain conditions and participate in repairing nerve function, a process called neurogenesis. Proliferative cells are found in the dentate gyrus of the hippocampus post-ICH, contributing to neuronal differentiation and recovery of neurological function (Zhu et al. 2018). In our study, Nissl staining showed fewer surviving neurons in the CA1 region of ICH rats compared with controls. NSC 87877 treatment was capable of rescuing the neuronal survival post-ICH. However, the further potential mechanism of the Nogo-A/PirB/TrkB signaling pathway in

destroying hippocampal neurons after ICH should be investigated.

Some shortcomings of this study should be noted. First, the in vivo ICH model was constructed using male adult rats. In clinical practice, the incidence of SBI post-ICH remains high in the elderly and females. Further explorations should be performed using female or elderly rats as animal models. Second, in-depth studies on the specific molecular mechanism of Nogo-A/PirB/TrkB axis are required, not only in neurons but also in other types of nerve cells.

In conclusion, we verified the inhibiting effect of the Nogo-A/PirB/TrkB pathway on ICH-induced cognitive dysfunction, neuronal apoptosis, and axonal regeneration. Thus, Nogo-A/PirB/TrkB could be a potential therapeutic target for the clinical treatment of ICH-induced brain injury.

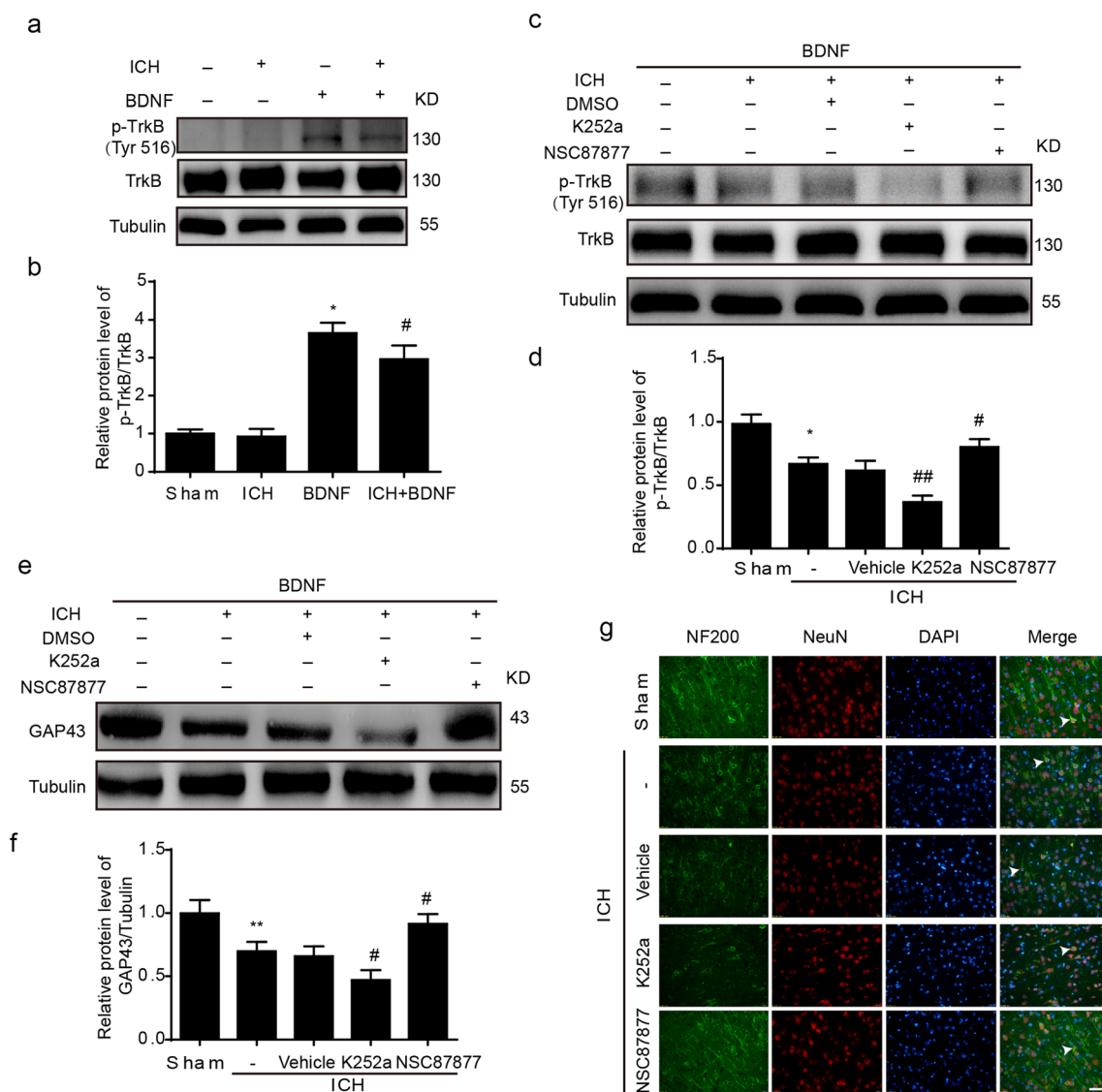


Fig. 6 Nogo-A/PirB/TrkB signaling pathway activation inhibited axon regeneration after ICH. **a** Protein levels of p-Tyr and TrkB in the rat brain. Tubulin served as the loading control. **b** Relative protein level of p-Tyr/TrkB. * $P < 0.05$, BDNF group compared with the sham group; # $P < 0.05$, ICH + BDNF group compared with the BDNF group. **c** Protein levels of p-Tyr and TrkB in rat brains of different groups. Tubulin served as the loading control. **d** Relative protein level of p-Tyr/TrkB. * $P < 0.05$, ICH group compared with the sham group; ## $P < 0.01$, ICH + K252a group

compared with the ICH + vehicle group; # $P < 0.05$, ICH + NSC 87877 group compared with the ICH + vehicle group. **e** Protein level of GAP43 in rat brain of different groups. Tubulin was served as the loading control. **f** Relative protein level of GAP43. ** $P < 0.01$, ICH group compared with the sham group; # $P < 0.05$, # $P < 0.05$, ICH + K252a group and ICH + NSC 87877 group compared with the ICH + vehicle group. **g** Immunofluorescence analyses of NF200 (green), nucleus stained as DAPI (blue), and neurons (red). Scale bar = 50 μ m

Authors' Contributions J.W and X.F conceived and designed the study. Y.L and C.M performed the experiments and wrote the paper. H.L and H.S helped conduct the literature review. X.L and G.C reviewed and edited the manuscript. Yinlong Liu and Chao Ma contributed equally to this work. All authors read and approved the manuscript.

Funding Information This work was supported by the Project of Jiangsu Provincial Medical Innovation Team (No. CXTDA2017003), Suzhou Key Medical Centre (No. Szzx201501), Scientific Department of Jiangsu Province (No. BE2017656), Suzhou Government (No. LCZX201601), Youth Science Foundation of Suzhou China (No. KJXW2017038), Science and Technology - Basic Research Project of Medical and Health Application of Suzhou China (No. SYS2018089), and the National

Key R&D Program of China (No. 2018YFC1312600 & No. 2018YFC1312601).

Compliance with Ethical Standards

All procedures were approved by the Animal Protection Committee of Soochow University and were performed in accordance with the National Institutes of Health's guidelines on the care and use of animals and the Animal Research: Reporting In Vivo Experiments guidelines. All efforts were made to minimize animal suffering and the number of animals used.

Conflict of Interest The authors declare that they have no conflict of interest.

References

- Akbik F, Cafferty WB, Strittmatter SM (2012) Myelin associated inhibitors: a link between injury-induced and experience-dependent plasticity. *Exp Neurol* 235:43–52. <https://doi.org/10.1016/j.expneurol.2011.06.006>
- Allen JK et al (2018) Sustained Adrenergic Signaling Promotes Intratumoral Innervation through BDNF. *Induction* 78:3233–3242. <https://doi.org/10.1158/0008-5472.can-16-1701>
- Banerjee A, Paluh JL, Mukherjee A, Kumar KG, Ghosh A, Naskar MK (2018) Modeling the neuron as a nanocommunication system to identify spatiotemporal molecular events in neurodegenerative disease. *Int J Nanomedicine* 13:3105–3128. <https://doi.org/10.2147/ijn.s152664>
- Ehrman LA et al (2014) The protein tyrosine phosphatase Shp2 is required for the generation of oligodendrocyte progenitor cells and myelination in the mouse telencephalon. *J Neurosci* 34:3767–3778. <https://doi.org/10.1523/jneurosci.3515-13.2014>
- Eyal G et al (2018) Human cortical pyramidal neurons: from spines to spikes via models. *Front Cell Neurosci* 12:181. <https://doi.org/10.3389/fncel.2018.00181>
- Fang MS et al (2017) Omega-3PUFAs prevent MK-801-induced cognitive impairment in schizophrenic rats via the CREB/BDNF/TrkB pathway. *Journal of Huazhong University of Science and Technology Medical sciences = Hua zhong ke ji da xue xue bao Yi xue Ying De wen ban. Huazhong keji daxue xuebao Yixue Yingdewen ban* 37:491–495. <https://doi.org/10.1007/s11596-017-1762-4>
- Fujita Y, Endo S, Takai T, Yamashita T (2011) Myelin suppresses axon regeneration by PIR-B/SHP-mediated inhibition of Trk activity. *EMBO J* 30:1389–1401. <https://doi.org/10.1038/emboj.2011.55>
- Hijioka M et al (2017) Inhibition of leukotriene B4 action mitigates intracerebral hemorrhage-associated pathological events in mice. *J Pharmacol Exp Ther* 360:399–408. <https://doi.org/10.1124/jpet.116.238824>
- Jeong SR et al (2012) Hepatocyte growth factor reduces astrocytic scar formation and promotes axonal growth beyond glial scars after spinal cord injury. *Exp Neurol* 233:312–322. <https://doi.org/10.1016/j.expneurol.2011.10.021>
- Karuppagounder SS et al (2016) Therapeutic targeting of oxygen-sensing prolyl hydroxylases abrogates ATF4-dependent neuronal death and improves outcomes after brain hemorrhage in several rodent models. *Sci Transl Med* 8:328ra329. <https://doi.org/10.1126/scitranslmed.aac6008>
- Lan X, Han X, Li Q, Yang QW, Wang J (2017) Modulators of microglial activation and polarization after intracerebral haemorrhage. *Nat Rev Neurol* 13:420–433. <https://doi.org/10.1038/nrneurol.2017.69>
- Lei C, Wu B, Liu M, Tan G, Zeng Q (2016) Pathogenesis and subtype of intracerebral hemorrhage (ICH) and ICH score determines prognosis. *Curr Neurovasc Res* 13:244–248
- Li N, Liu GT (2010) The novel squamosamide derivative FLZ enhances BDNF/TrkB/CREB signaling and inhibits neuronal apoptosis in APP/PS1 mice. *Acta Pharmacol Sin* 31:265–272. <https://doi.org/10.1038/aps.2010.3>
- Li H et al (2018) Critical role for Annexin A7 in secondary brain injury mediated by its phosphorylation after experimental intracerebral hemorrhage in rats. *Neurobiol Dis* 110:82–92. <https://doi.org/10.1016/j.nbd.2017.11.012>
- Meldolesi J (2018) Neurotrophin Trk receptors: new targets for cancer therapy. *Rev Physiol Biochem Pharmacol* 174:67–79. https://doi.org/10.1007/112_2017_6
- National Research Council (2011) Guide for the care and use of laboratory animals, 8th edn. National Academies Press, Washington, DC
- Naylor RL et al (2002) A discrete domain of the human TrkB receptor defines the binding sites for BDNF and NT-4. *Biochem Biophys Res Commun* 291:501–507. <https://doi.org/10.1006/bbrc.2002.6468>
- Osborne A et al (2018) Neuroprotection of retinal ganglion cells by a novel gene therapy construct that achieves sustained enhancement of brain-derived neurotrophic factor/tropomyosin-related kinase receptor-B signaling. *Cell Death Dis* 9:1007. <https://doi.org/10.1038/s41419-018-1041-8>
- Shen H et al (2015) Role of neurexin-1beta and neuroligin-1 in cognitive dysfunction after subarachnoid hemorrhage in rats. *Stroke* 46:2607–2615. <https://doi.org/10.1161/STROKEAHA.115.009729>
- Song M et al (2015) Slitrk5 mediates BDNF-dependent TrkB receptor trafficking and signaling. *Dev Cell* 33:690–702. <https://doi.org/10.1016/j.devcel.2015.04.009>
- Syken J, Grandpre T, Kanold PO, Shatz CJ (2006) PirB restricts ocular-dominance plasticity in visual cortex science (New York, NY) 313: 1795–1800 <https://doi.org/10.1126/science.1128232>
- Tan C, Yu C, Song Z, Zou H, Xu X, Liu J (2017) Expression of microRNA-29a regulated by Yes-associated protein modulates the neurite outgrowth in N2a cells 2017:5251236 10.1155/2017/5251236
- Tsai SY et al (2007) Intrathecal treatment with anti-Nogo-A antibody improves functional recovery in adult rats after stroke. *Exp Brain Res* 182:261–266. <https://doi.org/10.1007/s00221-007-1067-0>
- Urday S et al (2015) Targeting secondary injury in intracerebral haemorrhage—perihematomal oedema. *Nat Rev Neurol* 11:111–122. <https://doi.org/10.1038/nrneurol.2014.264>
- Wang F et al (2007) Nogo-A is involved in secondary axonal degeneration of thalamus in hypertensive rats with focal cortical infarction. *Neurosci Lett* 417:255–260. <https://doi.org/10.1016/j.neulet.2007.02.080>
- Wang Z, Wu L, You W, Ji C, Chen G (2013) Melatonin alleviates secondary brain damage and neurobehavioral dysfunction after experimental subarachnoid hemorrhage: possible involvement of TLR4-mediated inflammatory pathway. *J Pineal Res* 55:399–408. <https://doi.org/10.1111/jpi.12087>
- Wang Z et al (2017) Identification of two phosphorylation sites essential for annexin A1 in blood-brain barrier protection after experimental intracerebral hemorrhage in rats. *J Cereb Blood Flow Metab : Off J Int Soc Cereb Blood Flow Metab* 37:2509–2525. <https://doi.org/10.1177/0271678X16669513>
- Wilson TJ (2018) Novel uses of nerve transfers neurotherapeutics. *J Am Soc Exp NeuroTherapeutics*. <https://doi.org/10.1007/s13311-018-0664-x>
- Xi G, Strahle J, Hua Y, Keep RF (2014) Progress in translational research on intracerebral hemorrhage: is there an end in sight? *Prog Neurobiol* 115:45–63. <https://doi.org/10.1016/j.pneurobio.2013.09.007>
- Yiu G, He Z (2006) Glial inhibition of CNS axon regeneration. *Nat Rev Neurosci* 7:617–627. <https://doi.org/10.1038/nrn1956>
- Zhang JC et al (2014) Antidepressant effects of TrkB ligands on depression-like behavior and dendritic changes in mice after inflammation. *Int J Neuropsychopharmacol* 18. <https://doi.org/10.1093/ijnp/pyu077>
- Zhou Y, Wang S, Li Y, Yu S, Zhao Y (2017) SIRT1/PGC-1alpha signaling promotes mitochondrial functional recovery and reduces apoptosis after intracerebral hemorrhage in rats. *Front Mol Neurosci* 10: 443. <https://doi.org/10.3389/fnmol.2017.00443>
- Zhu W et al (2018) Changes in motor function, cognition, and emotion-related behavior after right hemispheric intracerebral hemorrhage in various brain regions of mouse. *Brain Behav Immun* 69:568–581. <https://doi.org/10.1016/j.bbi.2018.02.004>

Publisher's Note Springer Nature remains neutral with regard to jurisdictional claims in published maps and institutional affiliations.